Hysteresis in DNA compaction by Dps is described by an ising model

Vtyurina, Natalia N.; Dulin, David; Docter, Margreet W.; Meyer, Anne S.; Dekker, Nynke H.; Abbondanzieri, Elio A.

DOI
10.1073/pnas.1521241113

Publication date
2016

Document Version
Accepted author manuscript

Published in
Proceedings of the National Academy of Sciences of the United States of America

Classification:

- Biological Sciences, Biochemistry.

Title: An Ising model describes hysteresis in the process of DNA compaction by Dps

Short title: Ising-type hysteresis in DNA-protein complexes

Author affiliation: Natalia N. Vtyurina*, David Dulin*§, Margreet W. Docter*, Anne S. Meyer*, Nynke H. Dekker*, and Elio A. Abbondanzieri*

*Department of Bionanoscience, Kavli Institute of Nanoscience, Delft University of Technology, Lorentzweg 1, 2628 CJ, Delft, The Netherlands

§Current address: Biological Physics Research Group, Clarendon Laboratory, Department of Physics, University of Oxford, Parks Road, Oxford, OX1 3PU, UK

Corresponding author: Elio A. Abbondanzieri, Lorentzweg 1, 2628 CJ, Delft, The Netherlands, +31 (0)15-278-9245, e.a.abbondanzieri@tudelft.nl

Keywords: DNA condensation, cooperativity, hysteresis, Ising model, Dps, bacterial stress response, nucleoid associated protein

Author contributions: E.A.A. designed the research; N.N.V., D.D., N.H.D., and E.A.A. designed the single-molecule experiments; A.S.M contributed to the biochemical protocols; D.D. and M.W.D. provided analytical tools; N.N.V. performed the research and analyzed the data; N.N.V., D.D., N.H.D., and E.A.A. wrote the paper.

Abstract

In all organisms, DNA molecules are tightly compacted into a dynamic three-dimensional nucleoprotein complex. In bacteria, this compaction is governed by the family of nucleoid-associated proteins (NAPs). Under conditions of stress and starvation, a NAP called Dps (*DNA-binding protein from starved cells*) becomes highly upregulated and can massively reorganize the bacterial chromosome. Although static structures of Dps-DNA complexes have been documented, little is known about the dynamics of their assembly. Here, we employ fluorescent microscopy and magnetic-tweezers measurements to resolve the process of DNA compaction by Dps. Real-time *in vitro* studies demonstrated a highly cooperative process of Dps binding characterized by an abrupt collapse of the DNA extension, even under applied tension. Surprisingly, we also discovered a reproducible hysteresis in the process of compaction and decompaction of the Dps-DNA complex. This hysteresis is extremely stable over hour-long timescales despite the rapid binding and dissociation rates of Dps. A modified Ising model is successfully applied to fit these kinetic features. We find that long-lived hysteresis arises naturally as a consequence of protein cooperativity in large complexes and provides a useful mechanism for cells to adopt unique epigenetic states.

Significance Statement

Cooperativity has been a fundamental concept in our understanding of biological systems for over one hundred years. Here, we describe the observation of cooperative binding that exhibits long-lived hysteresis and cannot be described by a standard Hill model. Inspired by the Ising model of ferromagnetism, we describe this hysteresis as a consequence of cooperative binding in the limit of large complexes. We provide a method to relate the amount of hysteresis to the strength of the neighboring interactions between bound proteins and DNA. This novel kinetic feature of macromolecular complexes allows cells to create a binary response to small changes in external conditions and causes complexes to retain a memory of past conditions over long timescales.

\body

Introduction

Purified DNA behaves as an entropic spring spread out over a radius of gyration that scales as a function of the contour length (1). In contrast, DNA *in vivo* is highly organized and condensed. In bacteria, this condensation is caused by nucleoid-associated proteins (NAPs) that collectively shape the chromosome (2, 3). NAPs are capable of binding genomic DNA and in doing so alter its shape, control the transcriptional expression of genes, and remodel the structure of the nucleoid in response to external stimuli (2, 3).

Dps is an NAP structurally related to ferritins and associated with the response to stress. Dps is highly expressed in stationary phase (4-7) and is also involved in the cellular response to oxidative (4, 8-10), UV (8, 11), thermal (8), and pH shocks (8). In addition, Dps has been implicated in biofilm formation and tolerance to bacteriophage attacks (12). Dps monomers have a molecular mass of 19 kDa and assemble into a dodecameric shell **(Fig.1A)** (13). The resulting complex binds to both supercoiled and linear DNA to form a dense biocrystal structure (4, 7, 9, 14).

While the crystal structure of the Dps dodecamer has been solved (13), no atomic scale structure of Dps-DNA assemblies currently exists and little is known about complex formation. The affinity of Dps for DNA is very sensitive to buffer conditions. Like many DNA-binding proteins, Dps binds DNA more weakly in the presence of higher salt concentrations. Less typically, divalent cations such as Mg^{2+} can substantially weaken the affinity of Dps for DNA (9, 15). It has been proposed that fluctuations in divalent cation concentrations act as a trigger for biocrystal assembly *in vivo* (9, 16). Dps dodecamers have an overall negative surface charge that electrostatically repels the DNA backbone, while positively charged lysine residues located in the disordered N-termini play an important role in DNA binding (10, 13, 15). Interestingly, in images of biocrystals, Dps dodecamers are also tightly packed implying existence of extensive Dps-Dps interactions (14).

The transition into a compact Dps-DNA state appears to be cooperative (10), but the mechanism behind this transition is unclear. In bulk gel shift assays, Dps forms a massive complex with DNA and shows few intermediate sized complexes (15). Similarly, little evidence of structural intermediates has been reported in AFM and EM studies performed *in vitro*. Here we follow Dps-mediated DNA compaction (and subsequent decompaction) at the single-molecule level in real time. These experiments provide a detailed view of Dps binding transitions. Our measurements indicate that Dps-DNA complexes shift rapidly between two

stable states: compact/bound and extended/unbound with distinct hysteresis that can be fit using an Ising model.

Results

DNA compaction by Dps occurs abruptly. We developed a novel fluorescence assay to directly visualize the process of Dps-DNA complex formation at the single-molecule level without applied tension. Linear DNA molecules were attached to the surface of a flow cell and were labeled with YOYO-1 **(Fig.1B, green stars)**. To induce DNA compaction, a reaction buffer with 0.2 μM Dps labeled with Cy5 **(Fig.1B, red stars)** was added **(Materials and Methods)**.

We followed the binding of Dps proteins onto DNA molecules over tens of minutes using fluorescent microscopy **(Movie S1 in *SI Appendix*)**. We deliberately chose low Dps concentrations, as determined by a bulk gel shift assay **(*SI Appendix*, Fig.S1)**, to slow down the arrival of Dps and resolve the process of DNA compaction in real time. A sequence of frames for one such DNA molecule is shown in **Fig.2A**. Initially, the DNA molecule moved freely around the attachment point (0-720 s). The binding of Dps to the DNA (frames 900-1620 s) resulted in a rapid co-localization of these two molecules into a smaller, immobile Dps-DNA complex. To further analyze the transition of the DNA into an immobile state, we measured the fluctuations of the DNA between frames and the maximum fluorescence intensity of the Dps in individual complexes **(Fig.2B)**. We attribute the uniform increase in Dps brightness and abrupt decrease in DNA fluctuations to the binding of labeled Dps and compaction of the DNA. For each DNA molecule, a variable delay of 200 ± 230 s **(mean ± SD)** was observed prior to the collapse **(*SI Appendix,* Fig.S2A)**. In order to visualize the compaction at high time resolution, we aligned the traces at the time point of collapse **(*SI Appendix*, Fig.S2B)**. An averaged trace for all observed molecules after alignment shows that the majority of Dps molecules bound in a 6 s window, with DNA compaction occurring nearly simultaneously **(Fig.2C)**. This sharp transition suggests a highly cooperative binding mechanism and a tight coupling between Dps binding and the compaction of DNA.

DNA reorganization by Dps is history-dependent. Once Dps has assembled on DNA, we were interested in observing the dissociation of the Dps-DNA complex as well. We therefore analyzed five consecutive records of DNA molecules in the absence and presence of Dps

under different ionic conditions. We first measured the average fluctuations of DNA molecules in the absence of Dps **(Fig.2D, DNA only)**. Addition of 0.75 μM Dps in the reaction buffer resulted in a compaction of the DNA molecules (i.e. decreased fluctuations) and an abrupt increase of the peak Dps fluorescence **(Fig.2D, Flush in Dps)**. Upon flushing out Dps with 5 volumes of reaction buffer, we observed that the Dps intensity decreased but the Dps-DNA complexes remained a static structure **(Fig.2D, Flush out Dps)**. Addition of 3 mM $MgCl_2$ to the buffer weakened the affinity of Dps for DNA. This caused a sharp drop in Dps fluorescence intensity and a marked increase in DNA fluctuations, indicating the release of Dps from the DNA **(Fig.2D, Flush in $MgCl_2$)**. Subsequent removal of the $MgCl_2$ by flushing in 5 additional volumes of the reaction buffer demonstrated that the DNA remained flexible **(Fig.2D, Flush out $MgCl_2$)**. Dps could also be released by raising the pH to 8.1 **(*SI Appendix*, Fig.S2C)**.

In these experiments, preformed Dps-DNA complexes remain stable even after we lowered the Dps concentration to below 0.075 μM by flushing the flow cell with buffer (this estimation was made based on the reduction in the fluorescent background). In contrast, initially bare DNA did not collapse even after the addition of up to 0.1 μM Dps **(Movie S2 in SI Appendix)**. These experiments establish that DNA compaction by Dps is history-dependent rather than being a simple function of the current Dps concentration. In order to probe this hysteresis in more detail, we decided to use tension to perturb Dps-DNA assemblies.

Tension modulates the affinity of Dps for DNA. We developed a magnetic tweezer assay (17-19) that allowed us to modulate the force applied to individual DNA molecules in the presence of Dps **(Fig.1C)**. By applying a slowly decreasing force (from 15 to 0.01 pN over >40 min) followed by a slowly increasing force (from 0.01 to 15 pN over >40 min) we probed for hysteresis between the assembly and disassembly of Dps-DNA complexes **(Materials and Methods)**.

First, we consider the force-extension curves when the force is gradually decreased. For DNA molecules without Dps in the solution **(black solid line, Fig.3A)**, the measured extension at a given force can be approximated by the worm-like chain (WLC) model **(grey solid line, Fig.3A)** (20). In contrast, for DNA molecules in the presence of 8 μM Dps, a sharp compaction of the DNA is observed. Three example DNA traces **(blue, orange and green solid lines,**

Fig.3A) show an abrupt collapse that occurs at a critical force $F_1 \approx 1.5$ pN. This result demonstrates that the Dps molecules can perform work on the magnetic bead to compact DNA.

Next, we consider the force-extension curves when the force is gradually increased. Without Dps present, the DNA extension **(black dashed line, Fig.3A)** again follows the WLC model **(grey solid line, Fig.3A)**, as expected. However, in the presence of Dps the DNA extension follows a new pattern. The DNA molecules remain highly compacted until they reach a second critical force $F_2 \approx 6$ pN. At this force, the Dps-DNA complex breaks, and the DNA returns to the extension predicted by the WLC model **(blue, orange and green dashed lines, Fig.3A)**. We define F_1 and F_2 as the forces that correspond to a DNA extension of half the contour length (~3.5 μm) **(Fig. 3A)**.

Interestingly, in every recorded force-extension cycle in the presence of Dps we observe a distinct hysteresis in the DNA extension, with $F_2 > F_1$. In principle, this hysteresis could be a function of the pulling rate, as has been observed for RNA hairpins and other two-state systems near equilibrium (21, 22). However, additional experiments demonstrate that the observed hysteresis in our system is nearly independent of the pulling rate. First, we repeated the measurement with both a four-fold increase and a two-fold decrease in the pulling rate and observed essentially no change in the amount of hysteresis defined by F_1 and F_2 **(*SI Appendix*, Fig.S3A)**. Second, we performed experiments where we shifted from a high force ($F_{high} > F_2$) directly to an intermediate force ($F_1 < F_{int} < F_2$) and did not observe collapse of the DNA extension over the course of 30 min. Similarly, when we shifted from a low force ($F_{low} < F_1$) directly to the same intermediate force, the DNA remained stably collapsed for 30 min **(*SI Appendix*, Fig.S3B)**. Therefore, we conclude that under identical conditions the Dps-DNA complex can be trapped in one of two stable conformations, even on time scales exceeding the doubling time of bacteria.

To illustrate this behavior further, we replot the decreasing force-extension data from **Fig.3A** near the critical force F_1as a function of time **(Fig.3B)**. We observe that around F_1 the DNA extension decreased monotonically until it reached a fully compact state. We also replot the increasing force-extension data near the second critical force F_2 **(Fig.3C)**. The DNA extension exhibits an almost monotonic increase in extension until it is fully extended, indicating that DNA compaction is reversible. This result demonstrates that outside of the critical force

region, the DNA extension converges to a single equilibrium fairly rapidly, with hundreds of Dps dodecamers binding or releasing over the course of 200-300 s. We also note that on short timescales (~1 s) the DNA extension can exhibit small (< 50 nm) reversible fluctuations **(Fig.3B inset and 3C inset)**.

Plotting the average of multiple force-extension curves (N=11), we observe that the DNA extension is roughly homogeneous among the different molecules with a reproducible hysteresis **(Fig.3D)**. The variation of F_1 and F_2 between molecules ranged from 10-25% in different conditions. We attribute this variation to experimental uncertainty, since the actual force applied to beads across the field of view can vary by as much as 24% (23).

Dps-induced compaction of DNA is influenced by salt, magnesium, pH, and crowding conditions. When the applied force is lowered to F_1, Dps must do work on the bead to compact the DNA. Later, when the force is raised to $F_{2,}$ the bead must do work on the Dps to break the complex. The amount of work done in each case is a function of the strength of the Dps-DNA and Dps-Dps interactions. To explore how these interactions can be altered, we measured the compaction of DNA molecules exposed to Dps under a variety of buffer conditions. We performed force-extension cycles with the same pulling rate as shown in **Fig.3**, paying particular attention to shifts in the average of F_1 and F_2 and the total width of the hysteresis loop, defined as the difference between F_1 and F_2.

We recorded the compaction and decompaction of DNA at several Dps concentrations (2, 4, 8 μM). Surprisingly, varying the Dps concentration over this range yielded relatively minor changes in the mean values of F_1 and $F_{2,}$ and in the width of the hysteresis loop **(Fig.4A)**. Increasing the concentration of monovalent salts from 50 to 150 mM destabilized the Dps-DNA complex, as demonstrated by the progressive reduction of F_1 and F_2 and the narrowing of the width of the hysteresis loop **(Fig.4B)**. The addition of magnesium (2 mM) to the buffer caused a similar destabilization of the Dps-DNA complex **(Fig.4C)**. We also tested whether crowding can affect DNA compaction. Interestingly, the addition of PEG 8K caused a sharp increase in the stability of the Dps-DNA complex **(Fig.4D)**. Finally, we observed that increasing the pH weakened the Dps-DNA complex **(*SI Appendix*, Fig.S4)**. Overall, our results revealed that Dps-induced compaction and decompaction of DNA is strongly influenced by tension applied to the DNA, ionic strength, magnesium, macromolecular crowding, and pH.

These results are consistent with the trends observed in a recent single-molecule study of Dps-DNA interactions (24).

Discussion

Reversible DNA compaction by Dps is characterized by hysteresis. Here, we performed real-time *in vitro* measurements to study the biophysical properties of Dps-DNA complex formation at the single-molecule level. We find that a rate-limiting nucleation event stimulates the rapid incorporation of multiple Dps dodecamers on DNA, resulting in extensive compaction **(Fig.2A-C)**. Moreover, the degree of DNA compaction by Dps is influenced by past concentrations of Dps **(Fig.2D)**, i.e. the system exhibits hysteresis. By changing the tension applied to Dps-DNA complexes, we show that hysteresis is also observed in force-extension curves and can be characterized by the critical forces F_1 and F_2, which define the onset of DNA compaction and decompaction, respectively **(Fig.3)**. This hysteresis is nearly independent of the pulling rates ***(SI Appendix,* Fig.S3A*)***. Instead, we find that within the range of forces between F_1 and F_2 the DNA is trapped in one of the two stable local equilibria, i.e. compact or extended ***(SI Appendix,* Fig.S3B)**. Moreover, the measured hysteresis in the DNA extension is strongly affected by salinity, magnesium, crowding, and pH **(Fig.4 and *SI Appendix* Fig.S4)**. These data, combined with bulk gel shift assays **(*SI Appendix*, Fig.S1)**, demonstrate that Dps binds DNA cooperatively. Below we will explain why the observed hysteresis is a natural consequence of strong cooperativity in large systems.

Standard cooperativity models describe equilibrium distributions. We consider several possible models to explain the history-dependent mechanism of complex formation between a long, flexible polymer and a large number of self-interacting proteins. Cooperative binding is frequently modeled with the Hill equation (25). The resulting binding curve shows a characteristic sigmoidal shape that transitions sharply from low to high occupancy compared to a non-cooperative binding curve. The Hill equation has been used to characterize Dps binding previously (10), and it reasonably fits our own bulk experimental data **(*SI Appendix*, Fig.S1)**. However, the Hill model assumes that the system can equilibrate to find the global minimum in free energy, which precludes hysteresis. Other standard models of cooperativity, such as the Koshland-Némethy-Filmer (KNF) (26), Monod-Wyman-Changeux (MWC) (27), and Conformational Spread (CS) (28) models, can potentially be used

to model hysteresis, although almost all of the current literature focuses on their predictions at equilibrium. To better understand how a system can be trapped in non-equilibrium states, we turned to the Ising model of ferromagnetism.

A modified Ising model of cooperativity predicts hysteresis. The Ising model was first developed to describe interactions between magnetic dipoles that are arranged in an array and placed in an external magnetic field, giving rise to ferromagnetism (29)**.** In an idealized ferromagnetic system, a strong magnetic field can lock the dipoles predominantly in a single orientation, creating a stable magnetization that persists when the magnetic field is reduced. This is analogous to our observations that Dps can lock DNA in a stable complex that persists when the concentration of Dps is reduced or the tension is increased.

To apply the Ising model to Dps-DNA interactions, we assume that a DNA strand contains a fixed number of Dps binding sites, each of which can exist in an empty or occupied state. Further, we assume that Dps binding and DNA compaction at the binding site are tightly coupled, so that the number of occupied binding sites is proportional to the DNA extension. Our model depends on only two free parameters, which are defined in limiting cases. First, if the DNA is fully extended the affinity of Dps for DNA is characterized by a dissociation constant K_D. Second, we assume that additional Dps-Dps and Dps-DNA interactions stabilize the complex in compact states **(*SI Appendix*, Fig.S5A)**. If the DNA is fully compacted, the sum of all the energetic interactions between one dodecamer and its neighbors defines the cooperativity parameter I. For convenience we write I as a multiple of k_BT. Finally, for intermediate conformations some binding sites are empty, so the number of interactions between bound dodecamers will be lower than in the fully compacted conformation. Because the DNA can fold in many possible conformations, we cannot predict the exact number of interactions stabilizing a specific bound dodecamer. Instead, we use a mean-field approximation (30) to estimate that this number scales with the mean probability of Dps occupying the other binding sites. While the Ising model and the mean-field approximation have been applied to study cooperative binding in other systems (31), our approach focuses specifically on how these assumptions can give rise to hysteresis.

To model the effects of force, we set the size of each binding site to 60 base pairs of DNA based on titration measurements of Dps dodecamers (15). Compaction of these 60 base pairs by Dps decreases the DNA extension by a distance $\delta(F)$ that is dependent on the force

applied to the DNA molecule (20). Taken together, these parameters give rise to a transcendental equation for the probability P of a given DNA binding site being occupied by a Dps dodecamer **(*SI Appendix,* eq.[s8])**:

$$P([A],F) = \frac{1}{1+\frac{K_D}{[A]}e^{FD-PI}} = \frac{1}{1+\frac{K_{eff}}{[A]}e^{FD-(P-0.5)I}}. \qquad [1]$$

Here, $[A]$ is the concentration of Dps, F is the applied force, $D = \frac{\delta(F)}{k_BT}$ is the normalized change in extension, and $K_{eff} = K_D e^{-I/2}$ is the Dps concentration associated with 50% occupancy of the binding sites at zero force. The dimensionless parameter I is analogous to the Hill coefficient and serves a measure of cooperativity, while K_D describes how tightly Dps binds bare DNA.

To understand why our model gives rise to hysteresis we examine a concentration where the binding sites are equally likely to be occupied or empty ($[A] = K_{eff}e^{FD}$). When no cooperativity exists ($I = 0$), each binding site has an independent chance of being occupied, much like an individual coin toss. Therefore, if we plot the global free energy as a function of the number of bound dodecamers, it scales with the logarithm of the binomial distribution, creating an entropic minimum at $P = 0.5$ **(Fig.5A; *SI Appendix* eq.[s17])**. When $I > 0$, a quadratic term is added to the global free energy proportional to $\frac{1}{2}IP(1-P)$, penalizing states near $P = 0.5$. At the critical value of $I = 4$ the solution at $P = 0.5$ switches from a stable equilibrium to an unstable equilibrium. For values of $I > 4$ a global energetic barrier arises between the majority bound/unbound states, and the Dps-DNA complex behaves collectively as a two-state system.

Before this transition to a two state system, the Dps-DNA complex reaches equilibrium at a rate of roughly $k_{eq} = k_{on} + k_{off}$, where k_{on} and k_{off} are the individual binding and dissociation rates of Dps dodecamers (represented by the small saw-tooth peaks in **Fig.5A**). After the transition, the rate will begin to scale as $k_{eq} = e^{-H}\left(k_{on} + k_{off}\right)$, where H is the height of the global energetic barrier in units of k_BT. Since H scales with both the number of binding sites N and with cooperativity I, for large Dps-DNA complexes (e.g. kilobases of DNA) even small changes in the cooperativity dramatically increase the barrier height. For the $\sim 300k_BT$ barrier shown in **Fig. 5A**, k_{eq} will be approximately 10^{130} times slower than k_{on} and k_{off}.

When the barrier at $P = 0.5$ is very high, it is more useful to calculate the local equilibria rather than the global equilibrium, since we are unlikely to observe transitions over the barrier. In a non-cooperative binding curve ($I = 0$), only one local equilibrium exists and P gradually increases as a function of Dps concentration **(Fig.5B, grey; *SI Appendix* eq.[s3])**. In a cooperative binding curve where the system can globally equilibrate, we expect P to increase sharply as a function of concentration **(Fig.5B, green; *SI Appendix* eq.[s4])**. However, our Ising model predicts that at $I > 4$ **(*SI Appendix* eq.[s10, s18])**, there is a region where three solutions for P exist for a given Dps concentration **(Fig.5B, red; *SI Appendix* eq.[s5])**. In this region, the high and low solutions represent stable local equilibria of the system. The intermediate solution is an unstable equilibrium that corresponds to the energetic barrier between the stable solutions. Therefore, our model predicts that Dps-DNA complexes can exist in either a highly compact or extended conformation depending on the path used to bring the concentration into the critical region.

Force-extension experiments measure cooperativity and hysteresis. Next, we consider the effects of a changing tension applied to the Dps-DNA complex. The relationship between DNA extension and applied force is plotted for no cooperativity, a modified Hill model, and the Ising model in **Fig.5C (grey, green and red respectively) (*SI Appendix* eq.[s6-s9])**. Similar to the case without tension, our model predicts the existence of two highly stable local equilibria and one unstable equilibrium within a critical range of forces between $F_1$and F_2. The path used to bring the DNA into the critical force range determines which equilibrium is adopted. Above F_2 the DNA has an extended conformation. As the force is decreased below F_2, the DNA remains trapped at the extended local equilibrium **(*SI Appendix,* Fig.S3B)**. However, below F_1 no extended equilibrium exists. Therefore, when the force is then dropped below F_1 the Dps-DNA complex rapidly transitions to a compact conformation. Similarly, a compact DNA molecule suddenly transitions to an extended conformation only when the force is increased above F_2. In terms of the global free energy calculations, critical forces F_1 and F_2 correspond to the forces where the energetic barrier between the stable equilibria vanishes **(*SI Appendix,* Fig.S5B and eq.[s19])**.

The critical forces F_1 and F_2 can be used to determine the model parameters I and K_D, provided we specify the size of the binding site $\delta(F)$. We estimate F_1 and F_2 by identifying where the DNA reaches 50% of its full extension (~3.5 μm) in the decreasing and increasing

force-extension curves. At each critical force, a Dps dodecamer that binds DNA performs a fixed amount of work $W = F \cdot \delta(F)$. We define W_{diff} as the difference in work performed by Dps at the two critical forces F_1 and F_2 and show that it is a function of the parameter I **(*SI Appendix* eq.[s11])**:

$$\frac{W_{diff}}{k_B T} = (F_2 \cdot D - F_1 \cdot D) = I\sqrt{1 - \frac{4}{I}} - 2\ln\left(\frac{1+\sqrt{1-\frac{4}{I}}}{1-\sqrt{1-\frac{4}{I}}}\right). \quad [2]$$

We can also define W_{ave}, the average of the work performed by Dps at the two critical forces F_1 and F_2, and show that it is given by **(*SI Appendix* eq.[s12])**:

$$\frac{W_{ave}}{k_B T} = \frac{(F_1 \cdot D + F_2 \cdot D)}{2} = \frac{I}{2} + \ln\left(\frac{[A]}{K_D}\right) = \ln\left(\frac{[A]}{K_{eff}}\right). \quad [3]$$

Next, we compare this model to our empirical findings. When we change the concentration of Dps, W_{diff} remains roughly constant, as predicted by **eq.[2]**. However, if we change the ionic strength of the buffer, we observe large changes in W_{diff}, indicating that I is influenced by electrostatic interactions between neighboring Dps molecules **(Fig.5D)**. We also find that W_{ave} can be roughly fit to a logarithmic function of Dps concentration as predicted by **eq.[3]** and exhibits a strong dependence on electrostatic interactions **(Fig.5E)**. The magnitude of the change in W_{ave} relative to W_{diff} requires that both I and K_D are dependent on salt concentration. Low salt leads to tighter binding on bare DNA and strengthens neighboring interactions between Dps dodecamers.

Having determined the model parameters I and K_D at each salt concentration, we compare three experimental force-extension curves **(Fig.5F, dashed lines)** to the predictions of our model **(Fig.5F, solid lines)**. Within the critical region between $F_1$and F_2, we observe that the experimental curves track one of the two stable solutions. Outside this critical region, we find the experimental curves converge to the single stable solution.

A quantitative summary of the interaction parameters I and K_D (as derived from W_{diff} and W_{ave}) for all buffer conditions tested is presented in **Table 1**. We find that the neighboring interactions are weakened dramatically by salt, magnesium, and increasing pH. This result emphasizes that electrostatics play an important role in the binding of Dps dodecamers to each other. Conversely, the addition of crowding agents strengthens the neighboring interactions. Given that macromolecular crowding favors complexes with a smaller exposed

surface area (32) this finding supports the idea that Dps dodecamers form a compact geometry on the DNA. The affinity of Dps for extended DNA, as measured by $\ln(K_D)$, is affected by buffer conditions in a similar manner to the neighboring interactions. Therefore the overall stability of the complex, as measured by W_{ave}, correlates with the amount of hysteresis, as measured by W_{diff} **(*SI Appendix,* Fig.S6)**.

Hysteresis in other models of cooperativity. To examine whether hysteresis is unique to an Ising mechanism, we compare our model to other models of cooperativity. The KNF model (26), like our model, assumes a tight coupling between the occupancy of the DNA binding site and its conformation. Unlike our model, the KNF model assumes cooperative interactions are mediated through the conformation of neighboring DNA binding sites rather than through Dps-Dps contacts. However, given that occupancy and conformation are tightly coupled, these two interpretations produce equivalent energetic predictions. Therefore, our model can be viewed as a modification of the KNF model tailored to the flexible geometry of the Dps-DNA system.

The MWC model makes a very different physical assumption, requiring a concerted switch between a completely extended and a completely compacted DNA molecule (27). This concerted switching is not a physically realistic model of DNA dynamics, which should be uncorrelated over distances larger than the persistence length. Nevertheless, like our model the MWC model would give rise to a large global energetic barrier between two local binding equilibria and, therefore, to hysteresis **(*SI Appendix,* Fig.S7A and eq.[s21])**.

The CS model (28) is also derived from the Ising model, but it contains as many as five free parameters (33) compared to the two used in our model. With these additional parameters, CS model can approximate the KNF model, the MWC model, or our own model when applied to a fixed lattice. The CS model assumes that the binding substrate exists in an explicit geometry, such as a 1D ring or a 2D lattice (33). Traditionally the CS model avoids a mean-field approximation, so for 2D and 3D lattices the global free energy and binding probability must be computed numerically rather than by deriving explicit equations (e.g. **eq.[1]**). In our system, there is no fixed lattice since the DNA can fold in many potential conformations. Therefore, an exact comparison of our model to the CS model is not possible. Instead we consider a fixed 3D lattice (27 binding sites) and demonstrate that both models predict hysteresis that arises at nearly the same amount of cooperativity **(*SI Appendix,* Fig.S7B)**. The

transition of the CS model into a hysteresis regime has been noted previously (28), but has only been explored in the 1D limit (34), where the mean field approximation breaks down.

We conclude that cooperativity can lead to hysteresis for a variety of mechanistic assumptions. However, we find our modified Ising model is particularly well-suited for modeling Dps-DNA complexes: it directly accounts for Dps-Dps interactions that are implied by the crystal structure (13), it provides an explicit prediction of the free energies and equilibria using a minimal set of free parameters, and it allows for partially collapsed states. Further, the mean field approximation allows our model to be applied easily to a range of systems that might also be fit with a KNF or CS model while remaining agnostic about the exact geometry of the lattice. This makes our model particularly attractive when the lattice structure is undefined or too complex to precisely calculate the intermediate states.

Implications of cooperative hysteresis. The hysteresis described here for Dps-DNA complexes could be advantageous to bacterial survival for several reasons. First, hysteresis might ensure that complex formation becomes binary, since our model predicts a range of intermediate binding probabilities associated only with the unstable binding equilibrium **(Fig.5)**. This property makes it possible for the bacteria to maintain a subcritical concentration of Dps without substantial DNA compaction. Small alterations in the pH, crowding, salinity, or magnesium concentration in the cell could then greatly increase the overall affinity of Dps for DNA, quickly inducing compaction and protecting the chromosome. Cooperative hysteresis also allows cells to maintain a memory of past conditions, therefore, cells may tailor their response to current stress conditions. For example, a previous report suggests that Dps mediates a phase transition allowing starved cells to guard against additional stresses more effectively (9). Further, a population of cells could engage in bet-hedging strategies through hysteresis, allowing otherwise identical cells to become locked into different states. The variety of responses of these cells to new stress conditions would be more robust than adopting a single response.

Given that hysteresis arises naturally from several models of cooperativity in the limit of large complexes, this behavior is likely to be observed in other systems as well. For example, other proteins that condense DNA could exhibit similar dynamics, providing a new mechanism for epigenetic regulation. Alternately, replication of some eukaryotic viruses requires many copies of self-interacting proteins to assemble into large viral factories (35).

Cooperative hysteresis could provide a useful gating mechanism to prevent premature assembly of these replication factories. More generally, any large protein complex could exhibit hysteresis in assembly, especially when a 2D or 3D lattice can be identified.

Materials and methods

Dps labelling. Plasmid encoding the *dps* gene pLysS pET17b dps 2-1 was modified to insert a cysteine at position 79 (T79C), then expressed and purified as described for wild-type Dps (***SI Appendix, Material and Methods***). Cy5 Maleimide (GE Healthcare) was incubated at room temperature for 45 min with Dps monomers at a molar ratio of 1:15 Dps monomer to dye in a buffer of 50 mM Hepes-KOH, 400 mM NaCl, 10% glycerol, 5 M GdmCl, pH 7.3. Labeled Dps was subsequently diluted 5x with unlabeled Dps. Then, the sample was dialyzed against 50 mM Hepes-KOH, 100 mM NaCl, pH7.3, resulting in a labelling efficiency of ~10% (~1 dye per Dps dodecamer). Labelling of Dps did not affect the binding affinity of Dps for DNA **(*SI Appendix*, Fig.S8)**. Taking into account the labelling efficiency of Dps, the concentrations used, and the penetration depth of the evanescent wave we calculated the fluorescence intensity per Dps dodecamer in the flow cell. Based on this calculation we estimated that 4 ± 1.6 (mean ± SD) Dps dodecamers are bound per 1 kbp of DNA.

Fluorescence microscopy – experimental configuration. Single-molecule fluorescence measurements were performed on a total internal reflection fluorescence microscope (IX81, Olympus). Cy5 and YOYO-1 molecules were excited using a 640 nm and 488 nm lasers, respectively (CMR-LAS-640-100-D, CMR-LAS-488-150, Olympus). Fluorescence signals of Cy5 and YOYO-1 were collected through an oil immersion objective (U Apochromat 150X TIRF, NA 1.45, Olympus) by exciting the sample with two lasers simultaneously in epi (488 nm) and TIRF (640 nm) modes.

A series of images with 100 ms exposure time were recorded at 1 Hz using dual EMCCD cameras (iXon 3 897, Andor Technology) with a TuCam adapter. The image series was read using custom-made Matlab (MathWorks) software. After a linear drift correction, the Cy5 and YOYO-1 signals were co-localized by summing intensities over all frames and finding the linear transformation between spot locations of Dps and DNA. Individual spots were selected and cropped (ROI of 30x30 pixels). For each ROI the positions of the center of mass of DNA fluorescence and the maximum fluorescence intensities of Dps were extracted.

Fluctuations in the DNA center of mass between frames were calculated. For measurements of DNA collapse, records were time-shifted so that the collapse occurred at t=0 and a 5-point median filter was applied to the DNA fluctuation data. Records were then averaged over many molecules.

Magnetic tweezers – experimental configuration. The magnetic tweezers apparatus used in this study has been described previously (17-19). Briefly, light transmitted through the sample was collected by an oil-immersion objective (CFI Plan 50XH, Nikon) and projected onto a 12-Mpixels CMOS camera (12M Falcon2, Teledyne Dalsa). The images were acquired at a frequency of 25 Hz. The magnetic field was generated by a pair of horizontally aligned permanent neodymium-iron-boron magnets (SuperMagnete) separated by a distance of 1 mm, vertically translated by a motorized stage (M-126.PD2, Physik Instrumente) above the flow cell. Images, collected by the camera, were processed in real-time to create records of the bead positions in Cartesian coordinates with a custom written software in C++, CUDA and LabView (National Instruments) (19). The forces experienced by the DNA tethers have previously been calibrated using a custom routine (17, 18).

Acknowledgments: We are grateful to Theo van Laar for the DNA construct preparation; Ilja Westerlaken, Anna Haagsma, and Vlad Karas for initial assistance in working with Dps; Zhongbo Yu, Mariana Kober, Richard Janissen, Orkide Ordu and Daniel Lam for help with the experimental configurations; and Jelmer Cnossen for assistance with magnetic tweezer software. We thank Yera Ussembayev for critically reading the manuscript. This work was supported by the Nanofront initiative of the Netherlands Organization for Scientific Research (NWO) and the Department of Bionanoscience of the Delft University of Technology.

References

1. Smith DE, Perkins TT, & Chu S (1996) Dynamical scaling of DNA diffusion coefficients. *Macromolecules* 29(4):1372-1373.
2. Dillon SC & Dorman CJ (2010) Bacterial nucleoid-associated proteins, nucleoid structure and gene expression. *Nat Rev Microbiol* 8(3):185-195.
3. Dorman CJ (2014) Function of nucleoid-associated proteins in chromosome structuring and transcriptional regulation. *Journal of molecular microbiology and biotechnology* 24(5-6):316-331.
4. Almiron M, Link AJ, Furlong D, & Kolter R (1992) A novel DNA-binding protein with regulatory and protective roles in starved Escherichia coli. *Genes & development* 6(12B):2646-2654.
5. Azam TA, Iwata A, Nishimura A, Ueda S, & Ishihama A (1999) Growth phase-dependent variation in protein composition of the Escherichia coli nucleoid. *J Bacteriol* 181(20):6361-6370.

6. Meyer AS & Grainger DC (2013) The Escherichia coli Nucleoid in Stationary Phase. *Adv Appl Microbiol* 83:69-86.
7. Frenkiel-Krispin D*, et al.* (2004) Nucleoid restructuring in stationary-state bacteria. *Mol Microbiol* 51(2):395-405.
8. Nair S & Finkel SE (2004) Dps protects cells against multiple stresses during stationary phase. *J Bacteriol* 186(13):4192-4198.
9. Frenkiel-Krispin D*, et al.* (2001) Regulated phase transitions of bacterial chromatin: a non-enzymatic pathway for generic DNA protection. *Embo J* 20(5):1184-1191.
10. Karas VO, Westerlaken I, & Meyer AS (2015) The DNA-Binding Protein from Starved Cells (Dps) Utilizes Dual Functions To Defend Cells against Multiple Stresses. *J Bacteriol* 197(19):3206-3215.
11. Kavita Algu VSCC, Ravinder S. Dhami, Dallas A. K. Duncan (2007) Dps confers protection of DNA sequence integrity in UV-irradiated Escherichia coli. *Journal of Experimental Microbiology and Immunology (JEMI)* 11:60-65.
12. Lacqua A, Wanner O, Colangelo T, Martinotti MG, & Landini P (2006) Emergence of biofilm-forming subpopulations upon exposure of Escherichia coli to environmental bacteriophages. *Appl Environ Microb* 72(1):956-959.
13. Grant RA, Filman DJ, Finkel SE, Kolter R, & Hogle JM (1998) The crystal structure of Dps, a ferritin homolog that binds and protects DNA. *Nat Struct Biol* 5(4):294-303.
14. Wolf SG*, et al.* (1999) DNA protection by stress-induced biocrystallization. *Nature* 400(6739):83-85.
15. Ceci P*, et al.* (2004) DNA condensation and self-aggregation of Escherichia coli Dps are coupled phenomena related to the properties of the N-terminus. *Nucleic Acids Res* 32(19):5935-5944.
16. Minsky A, Shimoni E, & Frenkiel-Krispin D (2002) Stress, order and survival. *Nat Rev Mol Cell Bio* 3(1):50-60.
17. Yu Z*, et al.* (2014) A force calibration standard for magnetic tweezers. *Review of scientific instruments* 85(12):123114.
18. Velthuis AJWT, Kerssemakers JWJ, Lipfert J, & Dekker NH (2010) Quantitative Guidelines for Force Calibration through Spectral Analysis of Magnetic Tweezers Data. *Biophys J* 99(4):1292-1302.
19. Cnossen JP, Dulin D, & Dekker NH (2014) An optimized software framework for real-time, high-throughput tracking of spherical beads. *Review of Scientific Instruments* 85(10):103712
20. Bustamante C, Marko JF, Siggia ED, & Smith S (1994) Entropic Elasticity of Lambda-Phage DNA. *Science* 265(5178):1599-1600.
21. Liphardt J, Onoa B, Smith SB, Tinoco I, & Bustamante C (2001) Reversible unfolding of single RNA molecules by mechanical force. *Science* 292(5517):733-737.
22. Collin D*, et al.* (2005) Verification of the Crooks fluctuation theorem and recovery of RNA folding free energies. *Nature* 437(7056):231-234.
23. De Vlaminck I, Henighan T, van Loenhout MT, Burnham DR, & Dekker C (2012) Magnetic forces and DNA mechanics in multiplexed magnetic tweezers. *PLoS One* 7(8):e41432.
24. Lee SY, Lim CJ, Droge P, & Yan J (2015) Regulation of Bacterial DNA Packaging in Early Stationary Phase by Competitive DNA Binding of Dps and IHF. *Sci Rep* 5:18146.
25. Barcroft J & Hill AV (1910) The nature of oxyhaemoglobin, with a note on its molecular weight. *J Physiol-London* 39(6):411-428.
26. Koshland DE, Nemethy G, & Filmer D (1966) Comparison of Experimental Binding Data and Theoretical Models in Proteins Containing Subunits. *Biochemistry-Us* 5(1):365-385.
27. Monod J, Wyman J, & Changeux JP (1965) On Nature of Allosteric Transitions - a Plausible Model. *J Mol Biol* 12(1):88-118.
28. Bray D & Duke T (2004) Conformational spread: the propagation of allosteric states in large multiprotein complexes. *Annu Rev Biophys Biomol Struct* 33:53-73.
29. Ising E (1925) Report on the theory of ferromagnetism. *Z Phys* 31:253-258.

30. Tome T & de Oliveira MJ (1990) Dynamic phase transition in the kinetic Ising model under a time-dependent oscillating field. *Phys Rev A* 41(8):4251-4254.
31. Agliari E, Barra A, Burioni R, Di Biasio A, & Uguzzoni G (2013) Collective behaviours: from biochemical kinetics to electronic circuits. *Sci Rep* 3:3458.
32. Zhou HX, Rivas G, & Minton AP (2008) Macromolecular crowding and confinement: biochemical, biophysical, and potential physiological consequences. *Annu Rev Biophys* 37:375-397.
33. Duke TA, Le Novere N, & Bray D (2001) Conformational spread in a ring of proteins: a stochastic approach to allostery. *J Mol Biol* 308(3):541-553.
34. Graham I & Duke TA (2005) Dynamic hysteresis in a one-dimensional Ising model: application to allosteric proteins. *Phys Rev E Stat Nonlin Soft Matter Phys* 71(6 Pt 1):061923.
35. de Castro IF, Volonte L, & Risco C (2013) Virus factories: biogenesis and structural design. *Cell Microbiol* 15(1):24-34.

Figure Legends

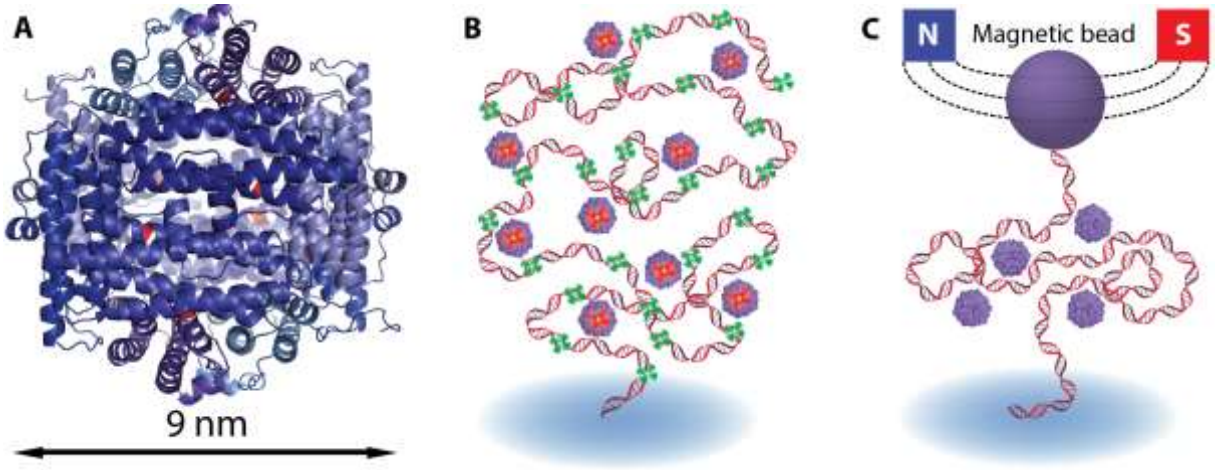

Fig.1. Dps spherical dodecamers bind to dsDNA. ***(A)*** Dps 12-mers form a shell-like structure 8-9 nm in diameter (13). Fluorescent dye is attached to a cysteine residue *(red)* facing a 4-5 nm internal cavity. ***(B)*** Cartoon of the fluorescent assay showing an immobilized DNA molecule labeled with YOYO-1 *(green stars)* and diffusing Dps dodecamers labeled with Cy5 *(red stars)*. ***(C)*** Cartoon of the magnetic tweezers assay showing a DNA molecule attached by one end to a microscope coverslip and by the other end to a magnetic bead. A pair of small permanent magnets controls the magnetic field.

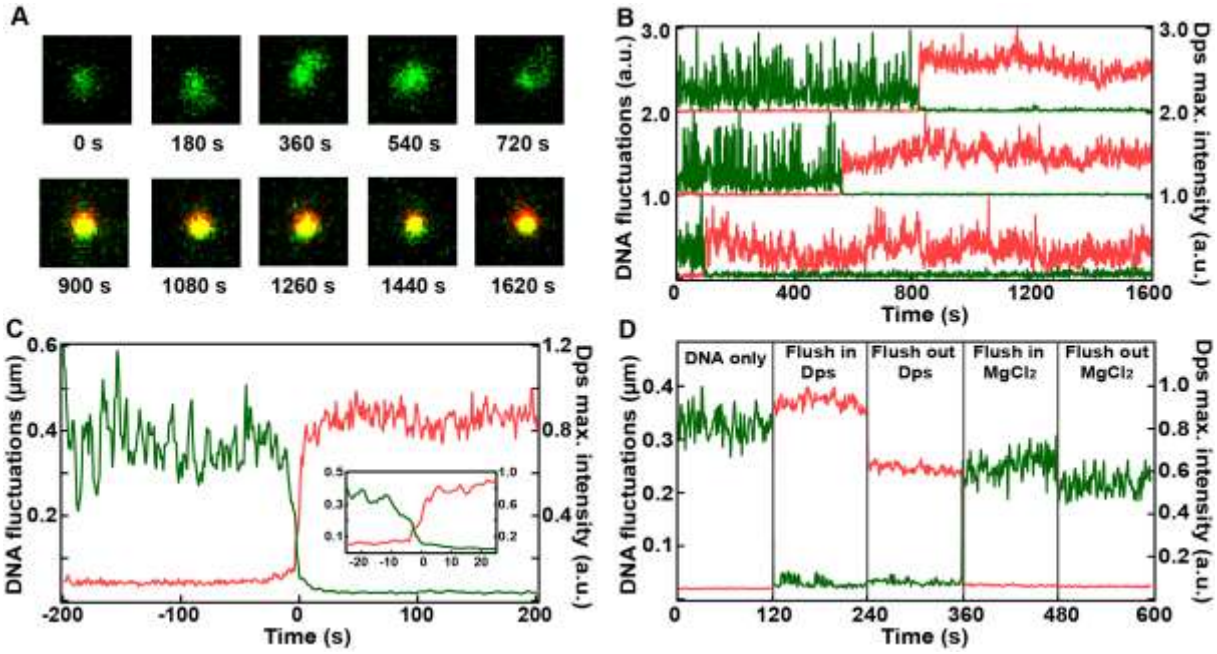

Fig.2. DNA compaction by Dps observed with fluorescence in real time. ***(A)*** Fluorescent images show a single DNA molecule *(green)* in the presence of 0.2 μM Dps undergoing thermal fluctuations in position (0-720 s). When Dps *(red)* binds to the DNA, these molecules co-localize into an immobile Dps-DNA complex (900-1620 s). ***(B)*** Three example traces show the abrupt decrease in DNA positional fluctuations between frames *(green)* and the sharp increase in the maximum fluorescence intensity of Dps *(red)* that define DNA compaction. ***(C)*** Individual records *(N=14)*, time-shifted so that collapse occurred at t=0, were averaged. The majority of Dps *(red)* bound and compacted the DNA (*green*) in less than 6 s. ***(D)*** Average DNA fluctuations *(green)* and Dps intensity *(red)* of a set of molecules (*N=53*) were recorded under five successive buffer conditions: DNA in reaction buffer without Dps (0-120 s); addition of 0.75 μM Dps (120-240 s); flushing with reaction buffer to remove Dps (240-360 s); addition of 3mM $MgCl_2$ (360-480 s); flushing with reaction buffer to remove $MgCl_2$ (480-600 s).

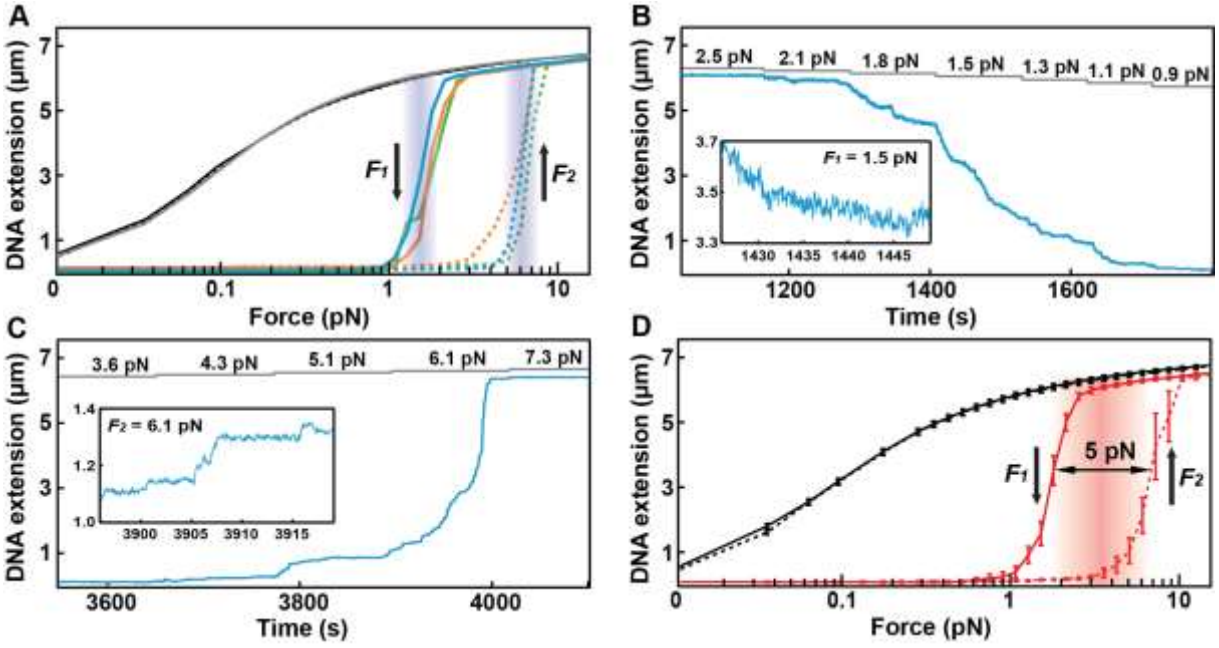

Fig.3. DNA force-extension cycles show hysteresis. ***(A)*** Force-extension curves for a DNA tether without Dps *(black)* and for three DNA tethers in the presence of 8 µM Dps *(blue, orange, green)*. The force-extension relationship of bare DNA is compared to the worm-like chain model *(grey)* (20). Solid lines correspond to decreasing force and dashed lines to increasing force. ***(B)*** Extension of a single DNA molecule (*blue*) plotted as a function of time as the force is decreased near the critical force F_1. Reversible fluctuations in the extension were limited to less than 100 nm (inset). The WLC extension *(grey)* is also plotted at each force. ***(C)*** Extension of the same DNA molecule plotted while the force is increased near the critical force F_2. ***(D)*** Average DNA extension *(N=11, mean, SEM)* in the absence *(black)* and presence *(red)* of 8 µM Dps. Solid lines correspond to decreasing force and dashed lines to increasing force. Hysteresis is demonstrated by the 5 pN gap between critical forces F_1 and F_2.

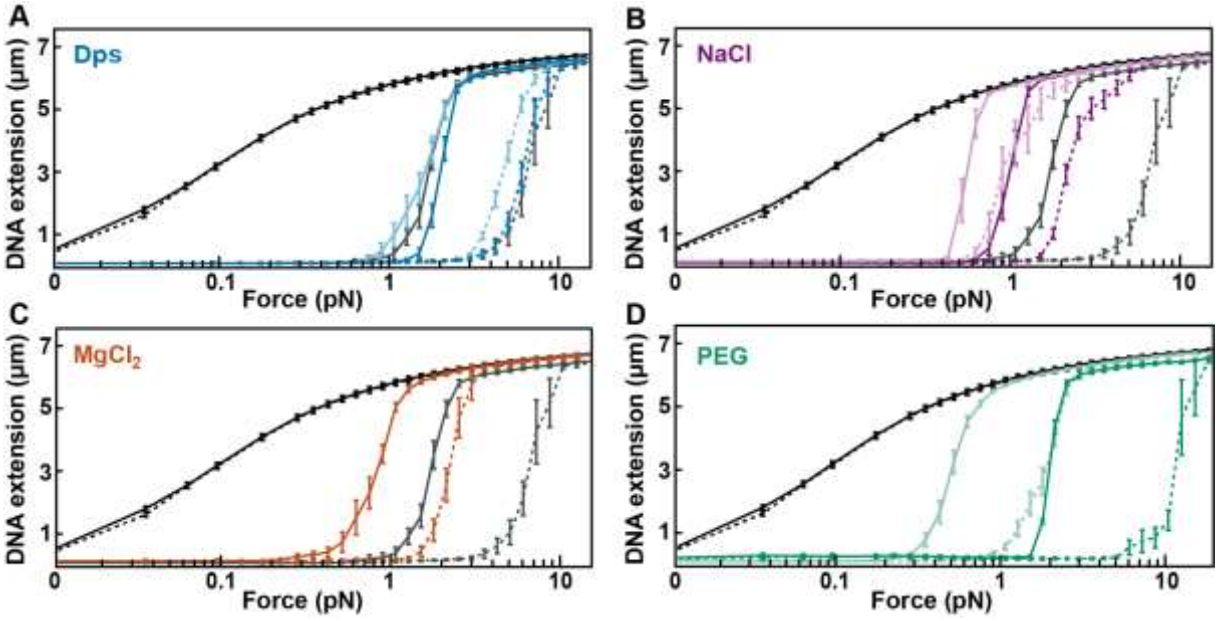

Fig.4. Buffer conditions affect DNA-Dps stability. Decreasing and increasing force records are represented by solid and dashed lines respectively. ***(A)*** Force-extension cycles with different Dps concentrations in the buffer: 2 µM *(light blue)*, 4 µM *(dark blue)* and 8 µM *(dark grey)* (50 mM NaCl, pH 7.3). ***(B)*** Force-extension cycles with different NaCl concentrations in the buffer: 50 mM *(dark grey)*, 100 mM *(dark purple)*, and 150 mM *(light purple)* (8 µM Dps, pH 7.3). ***(C)*** Force-extension cycles with different $MgCl_2$ concentrations in the buffer: 0 *(dark grey)* and 2 mM *(orange)* (8 µM Dps, 50 mM NaCl, pH 7.3). ***(D)*** Force-extension cycles with different 8K PEG concentrations (*w/v)* in the buffer: 0 *(light green)* and 5% *(dark green)* (0.5 µM Dps, 50 mM NaCl, pH 7.3). For all conditions we also recorded force-extension curves for bare DNA *(black)*, which did not vary significantly. Each curve is generated from the mean of 10 to 20 molecules and the error bars correspond to standard errors of the mean.

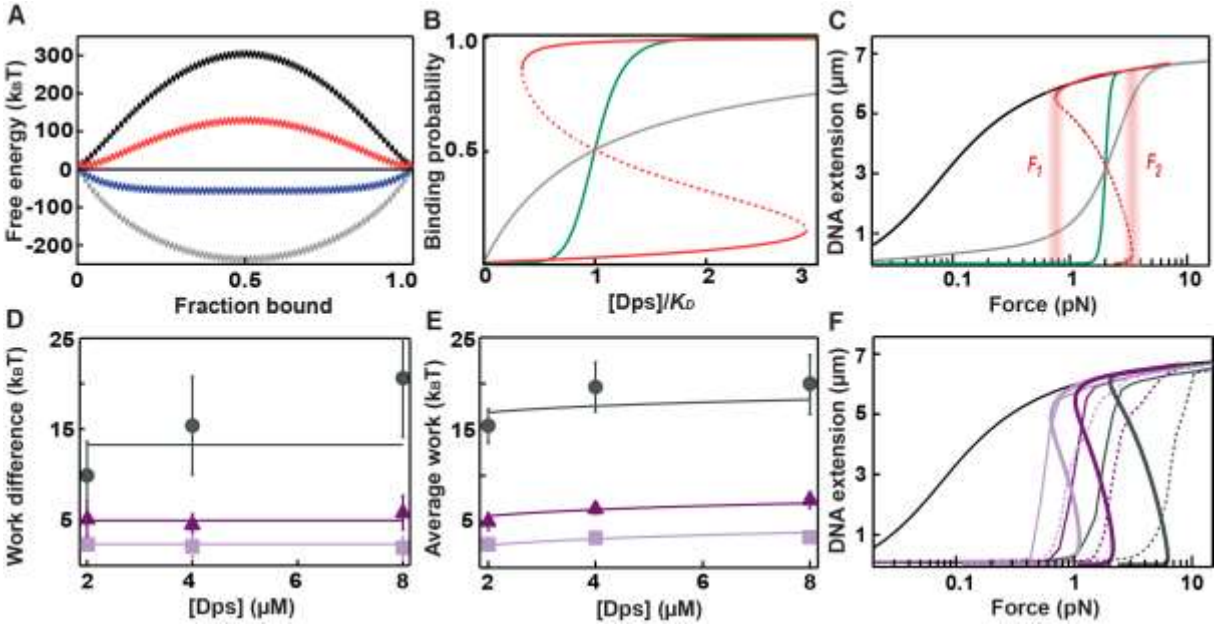

Fig.5. An Ising model describes hysteresis in DNA compaction by Dps. ***(A)*** Global free energy ΔG_{global} **(*SI* eq.[s17])** plotted as a function of bound Dps for various values of cooperativity parameter *G* demonstrates that high cooperativity creates two local equilibria: no cooperativity *I=0 (grey)*, $I = 4$ *(blue)*, $I = 8$ *(red),* and $I = 12$ *(black)*. ***(B)*** The probability of occupying a binding site on DNA as a function of the effective Dps concentration in the case of: no cooperativity *(grey)* **(*SI* eq.[s3])**, Hill cooperativity *($N_H = 8$, blue)* **(*SI* eq.[s4])** and Ising cooperativity *($I = 8$, red)* **(*SI* eq.[s5])**. ***(C)*** Force-extension predictions for Dps binding on DNA with different cooperative models: no binding *(black)*, non-cooperative *(grey)* **(*SI* eq.[s6], [s9])**, Hill *(blue)* **(*SI* eq.[s7],[s9])** and Ising *(red)* **(eq.[1]; *SI* eq.[s8], [s9])**. Sharp transitions can occur at critical forces F_1 (compaction) and F_2 (decompaction). ***(D)*** Work difference between F_1 and F_2 as function of Dps concentration for different NaCl concentrations (mean, SD): 50 mM *(dark grey circles)*, 100 mM *(dark purple triangles)* and 150 mM *(light purple squares)*. Experimental values were fit to **(eq.2; *SI* eq.[s11])** *(solid lines)*. ***(E)*** The average work between F_1 and F_2 as function of Dps concentration for different NaCl concentrations (mean, SD): 50 mM *(dark grey circles)*, 100 mM *(dark purple triangles)*, and 150 mM *(light purple squares)*. Experimental values were fit to **(eq.[3]; *SI* eq.[s12])** *(solid lines)*. ***(F)*** Simulated force-extension curves *(bold solid lines)* fit to the Ising model in comparison with the mean experimental data *(thin solid and dashed lines)* for different NaCl concentrations: 50 mM *(dark grey)*, 100 mM *(dark purple)*, and 150 mM *(light purple)* at 8 μM Dps.

Table 1. List of values for W_{diff}, W_{ave}, I, and $ln(K_D)$ derived from the Ising model for different buffer conditions (mean, SD).

		Work difference, K_BT	Work average, K_BT	Cooperativity, I	$\ln(K_D)$	Buffer condition
Dps, µM	**2**	15.38±03.69	15.38±1.84	23.62±4.05	-2.88±1.84	**NaCl=50 mM; $MgCl_2$=0; PEG=0; pH=7.3**
	4	20.61±5.41	19.63±2.70	29.30±5.83	-3.59±2.70	
	8	23.91±6.49	19.87±3.25	32.83±6.94	-1.37±3.25	
NaCl, mM	**50**	23.91±6.49	19.87±3.25	32.83±6.94	-1.37±3.25	**Dps=8 µM; $MgCl_2$=0; PEG=0; pH=7.3**
	100	5.82±1.87	7.34±0.93	12.74±2.26	1.11±0.93	
	150	1.86±1.31	3.25±0.66	7.61±1.97	2.63±0.66	
$MgCl_2$, mM	**0**	23.91±6.49	19.87±3.25	32.83±6.94	-1.37±3.25	**Dps=8 µM; NaCl=50 mM; PEG=0; pH=7.3**
	2	6.59±1.50	7.02±0.75	13.66±1.78	1.88±0.75	
PEG, %	**0**	6.77±1.45	5.52±0.73	13.87±1.72	0.72±0.73	**Dps=0.5 µM; NaCl=50 mM; $MgCl_2$=0; pH=7.3**
	5	46.83±8.76	32.46±4.38	56.87±9.09	-4.72±4.38	
pH	**6.9**	8.90±3.57	9.65±1.78	16.36±4.12	-0.78±1.78	**Dps=2 µM; NaCl=100 mM; $MgCl_2$=0; PEG=0**
	7.3	5.15±1.91	5.01±0.95	11.92±2.35	1.65±0.95	
	8.1	0.63±0.26	1.50±0.13	5.64±0.49	2.01±0.13	